Pergamon

Int. J. Heat Mass Transfer. Vol. 39, No. 2, pp. 311–317, 1996

0017-9310/96 $9.50 + 0.00

0017-9310(95)00122-0

The optimal spacing of cylinders in free-stream cross-flow forced convection

G. STANESCU,† A. J. FOWLER‡ and A. BEJAN†§

† Department of Mechanical Engineering and Materials Science, Duke University, Durham, NC 27708-0300, U.S.A.

‡ Mechanical Engineering Department, University of Massachusetts Dartmouth, North Dartmouth, MA 02747, U.S.A.

(*Received* 15 *August* 1994 *and in final form* 10 *March* 1995)

Abstract—This is an experimental, numerical and analytical study of the optimal spacing between cylinders in cross-flow forced convection. The cylinder array occupies a fixed volume and is exposed to a free stream of given velocity and temperature. The optimal cylinder-to-cylinder spacing is determined by maximizing the overall thermal conductance between all the cylinders and the free stream. In the first part, the optimal spacing and corresponding maximum thermal conductance are determined based on experiments with forced air for $H/D = 6.2$ and in the Re_D range 50–4000, where Re_D is based on the free-stream approach velocity and cylinder diameter D, and H is the array length in the flow direction. In the second part, similar results are developed based on numerical simulations for $Pr = 0.72$, $10 \leqslant H/D \leqslant 20$ and $40 \leqslant Re_D \leqslant 200$. In the concluding section, the experimental and numerical results for optimal spacing and maximum thermal conductance are explained and correlated analytically by intersecting the small-spacing and large-spacing asymptotes of the thermal conductance function.

INTRODUCTION

The development of cooling techniques for electronic packages is illustrated by the emergence of fundamental results that apply to entire classes of geometric configurations [1, 2]. Clear examples are the design rules for selecting the spacing between the geometric features of a package of fixed volume such that the overall thermal conductance between package and coolant is maximized. Optimal spacings have been reported already for several geometries, in both natural convection [3–6] and forced convection [7–13]. The objective of the present study was to determine the optimal spacing for another basic configuration: the array of cylinders with cross-flow forced convection. We did this work experimentally and numerically, and in the end we used scale analysis to organize the results in dimensionless form.

EXPERIMENTAL RESULTS

As shown in Fig. 1, the test section of the experimental apparatus was a bundle of cylindrical heaters mounted in a volume that was approximately the same in all the experiments. Bundles with 12, 14, 16 and 23 cylinders were tested with the flow oriented in the H direction. The corresponding spacings were $S/D = 1$, 0.75, 0.50 and 0.25. The spacing S is defined such that $S = 0$ when the cylinders touch. The cylinder diameter was fixed, $D = 6.35$ mm. End losses were minimized by holding the cylinders between two wooden walls separated by the distance $L = 134$ mm.

The cylindrical heaters were connected in parallel and powered by a variable autotransformer that produced voltages between 0 and 140 V. Each cylinder consisted of a helically wound heating element (resistance 96 Ω) held in a ceramic insulator fitted with conductive magnesium oxide. The outer cover was polished 304 stainless steel. As the heating was distributed uniformly throughout the array, the maximum temperature was registered on the trailing row of cylinders ($T_{w,1}$). The temperature was uniform (within 0.07°C) around the cylinder circumference: we found this by running the experiment with a single cylinder at $Re_D = 200$, and rotating the cylinder to change the circumferential position of the $T_{w,1}$ reading. The temperatures $T_{w,1}$, $T_{w,2}$ and T_∞ were measured half-way between the two wooden walls. Copper–constantan type T thermocouples referenced to an ice–water mixture were placed in 1 mm hemispherical depressions machined into the steel sheath of the heater.

At relatively high Reynolds numbers, $2000 \leqslant Re_D \leqslant 4000$, we tested only three of the bundles, $S/D = 0.25$, 0.5 and 0.75, because the optimal S/D ratio was always in the S/D range 0.25–0.75 (Fig. 2). The dimensions of the bundle cross-section varied slightly from one setup to the next, in order to accommodate an integral number of cylinders in a relatively fixed volume. The swept length H was equal to 39.2 mm within 2%, while the width W was equal to 33.4 mm within 7%. Each bundle was installed in the middle

§ Author to whom correspondence should be addressed.

NOMENCLATURE

c_p	specific heat at constant pressure	$\tilde{S}$	relative spacing, S/D
D	cylinder diameter	T	temperature
H	length in the flow direction, Fig. 1	T_w	cylinder surface temperature
k	thermal conductivity	T_∞	free-stream temperature
K	permeability of the array as a porous medium	u, v	velocity components
		$\tilde{u}, \tilde{v}$	dimensionless velocity components
L	cylinder length	U	volume averaged longitudinal velocity
$\dot{m}$	mass flow rate	U_∞	free-stream velocity
n	total number of cylinders	W	transversal dimension, Fig. 1
Nu_D	Nusselt number	x, y	Cartesian coordinates
p	pressure	$\tilde{x}, \tilde{y}$	dimensionless coordinates.
$\tilde{p}$	dimensionless pressure		
Pr	Prandtl number	Greek symbols	
q	total heat transfer rate	α	thermal diffusivity
q_1	heat transfer rate of a single cylinder	θ	dimensionless temperature
$\tilde{q}$	dimensionless overall thermal conductance	μ	viscosity
		ν	kinematic viscosity
Re_D	Reynolds number, $U_\infty D/\nu$	ρ	density
S	cylinder-to-cylinder spacing	φ	porosity.

of the test section of a suction-type wind tunnel. The test section was a 1.8 m long channel with a cross-section of 0.76 m (width) × 0.5 m (height). The free-stream velocity U_∞ was measured using a calibrated Pitot tube and an inclined manometer. The uncertainty in U_∞ was 2.5%.

At lower Reynolds numbers, $50 \leqslant Re_D \leqslant 200$, we tested the bundles with $S/D = 0.50$, 0.75 and 1, as shown in the lower part of Fig. 2. The test section of the suction-type wind tunnel used for this series was 0.9 m long, 0.134 m wide and 0.13 m tall. The bundle dimensions were $H = 39.2$ mm (within 2%) and $W = 35.2$ mm (within 12%). This time U_∞ was measured using a calibrated Taylor anemometer. The uncertainty in U_∞ was 0.58%.

The radiation contribution to the total heat transfer rate was estimated to be less than 0.2% for $2000 \leqslant Re_D \leqslant 4000$ and 1.5% for $50 \leqslant Re_D \leqslant 200$. This insignificant level is due to the moderate temperature of the cylinder surface: the highest temperature reading was 37.7°C, while the background temperature in the wind tunnel was 25°C.

We started each run by setting the voltage and current for the resistance heaters and the air free-stream velocity. We then waited for 2–4 h while monitoring the changes in voltage, current, $T_{w,1}$, $T_{w,2}$ and T_∞. We took final readings when the relative changes in voltage, current and temperature were less than 0.2, 0.2 and 0.06%, respectively. These relative changes were estimated by repeating the run for the same S/D and Re_D values, letting the run last 10 h. It is worth noting that these relative changes are small when compared with the uncertainties in the corresponding measurements.

The calculation of the dimensionless overall thermal conductance $\tilde{q}$, or volumetric heat transfer density,

$$\tilde{q} = \frac{q/(T_{w,1} - T_\infty)}{kHLW/D^2} \tag{1}$$

was based on measuring the power dissipated in all the heaters (q), the maximum temperature ($T_{w,1}$) and the free-stream temperature (T_∞). The air properties were evaluated at the film temperature $(T_w + T_\infty)/2$, where $T_w = (T_{w,1} + T_{w,2})/2$. The error analysis was based on the method of Kline and McClintock [14]. The estimated uncertainty in $\tilde{q}$ is between 5 and 8.8% when $2000 \leqslant Re_D \leqslant 4000$, and between 3.2 and 8.6% when $50 \leqslant Re_D \leqslant 200$. The uncertainty in Re_D is 3.2% in the high Re_D range and 2.1% in the low Re_D range. These estimates are also based on the following uncertainties: 0.5% in voltage and 1% in current, 1% in air thermal conductivity [15] and 2% in air viscosity [15].

Figure 2 summarizes the results from the 33 cases $(S/D, Re_D)$ investigated experimentally. These results show that the overall thermal conductance can be maximized by selecting the spacing or the number of cylinders. We curve fitted the data and found S_{opt}/D by solving $\partial\tilde{q}/\partial(S/D) = 0$. The S_{opt}/D results of this operation are shown in Fig. 3. The group used on the abscissa was determined based on an order-of-magnitude analysis designed to correlate on the same plot both the experimental and the numerical results. The maximum overall thermal conductance that corresponds to the optimal spacing is reported in Fig. 4.

NUMERICAL RESULTS

In the second phase of our study we simulated numerically the flow and heat transfer through the array at low Reynolds numbers, $40 \leqslant Re_D \leqslant 200$. It was shown in ref. [16] that in the laminar regime the

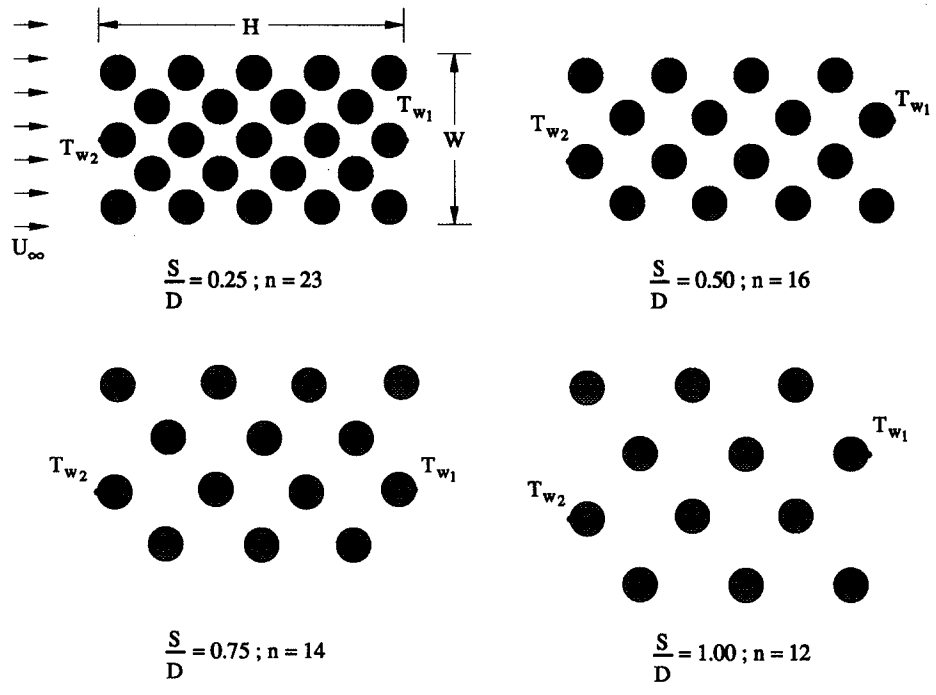

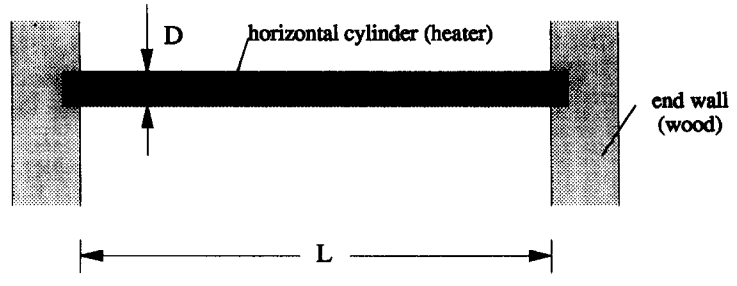

Fig. 1. The test section of the experimental apparatus.

flow through a large bank of cylinders can be simulated accurately by calculating the flow through a single channel, such as that illustrated in Fig. 5. Because of symmetry, there was no fluid exchange and no heat transfer between adjacent channels. The cylinders were arranged in an equilateral triangular array.

The mass, momentum and energy equations were simplified in accordance with the assumptions of two-dimensional steady-state flow with constant properties:

$$\frac{\partial u}{\partial x} + \frac{\partial v}{\partial y} = 0 \tag{2}$$

$$u\frac{\partial u}{\partial x} + v\frac{\partial u}{\partial y} = \nu\left(\frac{\partial^2 u}{\partial x^2} + \frac{\partial^2 u}{\partial y^2}\right) - \frac{1}{\rho}\frac{\partial p}{\partial x} \tag{3}$$

$$u\frac{\partial v}{\partial x} + v\frac{\partial v}{\partial y} = \nu\left(\frac{\partial^2 v}{\partial x^2} + \frac{\partial^2 v}{\partial y^2}\right) - \frac{1}{\rho}\frac{\partial p}{\partial y} \tag{4}$$

$$u\frac{\partial T}{\partial x} + v\frac{\partial T}{\partial y} = \alpha\left(\frac{\partial^2 T}{\partial x^2} + \frac{\partial^2 T}{\partial y^2}\right). \tag{5}$$

With reference to Fig. 5, the velocity components u and v are aligned with x and y, respectively. The computational domain contains the actual channel (flow length H) plus an upstream section and a downstream section. Accuracy tests showed that the calculated total heat transfer rate from the channel was relatively insensitive (with changes less than 1%) to further doubling of the upstream and downstream lengths.

The non-dimensionalization of equations (2)–(5) was based on recognizing that the parameter that does not change with S is the upstream velocity U_∞. Rela-

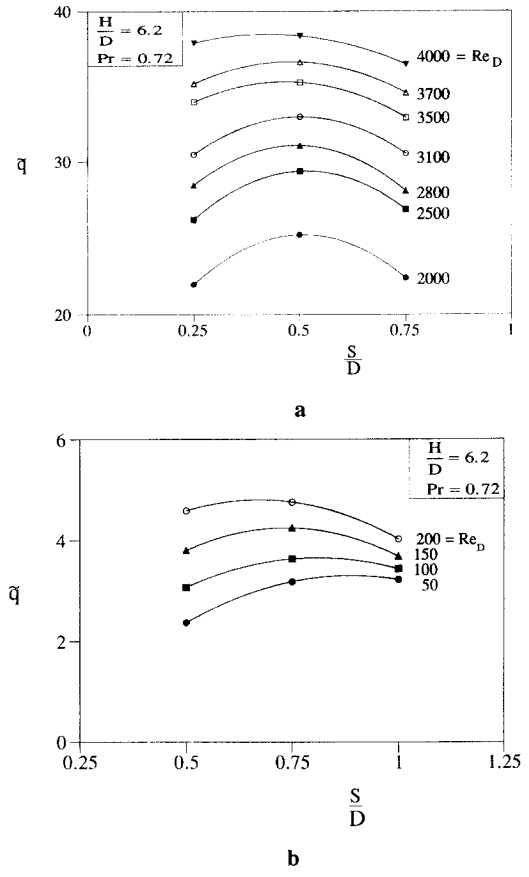

Fig. 2. Experimental results for the overall thermal conductance.

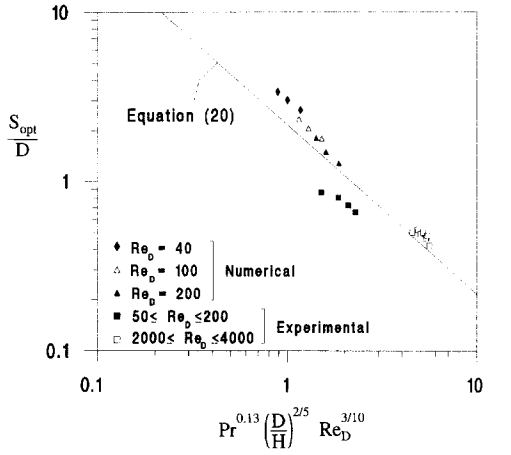

Fig. 3. The optimal cylinder-to-cylinder spacing for maximum overall thermal conductance: experimental, numerical and scaling results.

tive to the computational domain of Fig. 5, where the channel shown is one of a large number of identical channels stacked in the y direction (i.e. $W \gg D$), the fixed U_∞ means that the stagnation excess pressure at the channel entrance is fixed,

$$\Delta p \cong \tfrac{1}{2}\rho U_\infty^2. \tag{6}$$

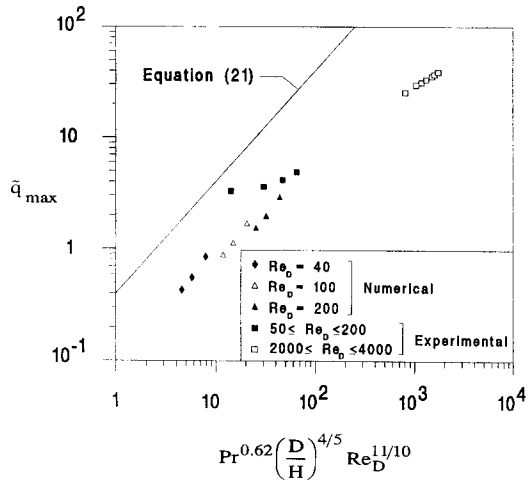

Fig. 4. The maximum overall thermal conductance: experimental, numerical and scaling results.

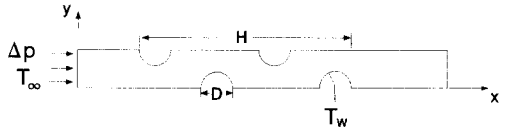

Fig. 5. Scale drawing of the computational domain for one fluid channel in an array of parallel cylinders in cross-flow.

This constraint captures the physics of the configuration optimized in the experiment, which is that larger S/D values permit larger flow rates through each channel, but smaller heat transfer contact area. The assumption in equation (6) is particularly good in the case of arrays with many cylinders in the flow direction ($H/D \gg 1$), which was the case in the present numerical simulations. The dimensionless variables used in reformulating equations (2)–(5) were:

$$(\tilde{u}, \tilde{v}) = (u, v)\left(\frac{\rho}{\Delta p}\right)^{1/2} \quad (\tilde{x}, \tilde{y}) = \frac{(x, y)}{D} \tag{7}$$

$$\tilde{p} = \frac{p}{\Delta p} \quad \theta = \frac{T - T_\infty}{T_w - T_\infty} \tag{8}$$

$$Pr = \frac{\nu}{\alpha} \quad Re_D = \frac{D}{\nu}\left(\frac{2\Delta p}{\rho}\right)^{1/2}. \tag{9}$$

The flow boundary conditions were: $\tilde{p} = 1$ at the inlet to the computational domain; zero normal stress at the outlet; free slip, no penetration at the fluid channel-to-channel interfaces (planes of symmetry) between two consecutive cylinders; no slip, no penetration at the cylinder surfaces; and free slip, no penetration on the longitudinal boundaries of the upstream and downstream sections. The temperature boundary conditions were $\theta = 1$ on the cylinder surfaces, and $\theta = 0$ at the inlet ($\tilde{x} = 0$). The remaining portions of the computational domain were modeled as adiabatic.

The system of equations was solved using a finite element package [17] and a combination of DEC 5000

workstations, DEC alpha workstations, and a CRAY C90. The larger H/D solutions required the use of a supercomputer due to the large amount of space occupied by temporary files created by the solver. The computational cost for the solutions was fairly small (90 s of C90 cpu time per solution), because the equations are weakly coupled. Grid refinement tests indicated that the solution was insensitive to further grid doubling (change in total heat transfer was less than 1%) if the velocity solution was generated on a grid with 20 nodes per unit D in the x and y directions, and the temperature solution was generated on a grid with 40 nodes per unit D in x and y. The velocity solution from the coarser grid was interpolated onto the finer grid before the temperature solution was calculated.

All the numerical solutions were developed for $Pr = 0.72$. The flow length of the array was fixed at three different values, $H/D = 10$, 15 and 20. Three flows were calculated for each H/D value, namely $Re_D = 40$, 100 and 200. These Re_D values were chosen because they resulted in Reynolds numbers based on channel mean velocity that ranged from 10 to approximately 100. Solutions for such Reynolds numbers greater than 100 would not have been accurate because our numerical formulation suppresses the waviness of the wakes in the transition regime between laminar and turbulent flow [18].

To find the optimal S/D for a given Re_D, we monitored the total heat transfer from the channel while varying the number of cylinders but holding H/D fixed. Note that the channel width (Fig. 5) also varied with the number of cylinders because the equilateral triangle arrangement did not change. The number of cylinders (or S/D) was varied until the dimensionless overall thermal conductance $\tilde{q}$ of equation (1) exhibited a maximum.

The results are illustrated in Fig. 6 for $H/D = 20$. The S_{opt}/D and $\tilde{q}_{max}$ values were refined by fitting the three highest $\tilde{q}$ points with a parabola and solving $\partial\tilde{q}/\partial(S/D) = 0$. The nine numerical data obtained in this manner have been added to the experimental data in Figs. 3 and 4. Worth noting is the good alignment of the numerical and experimental sets. The agreement is remarkable if we think that in the experiments the array was short ($H/D = 6.2$) and with uniform flux, while in the numerical simulations it was longer, infinitely wider and with isothermal cylinders. Together, the experiments and the numerical simulations cover a wider parametric domain, $6.2 \leqslant H/D \leqslant 20$ and $40 \leqslant Re_D \leqslant 4000$.

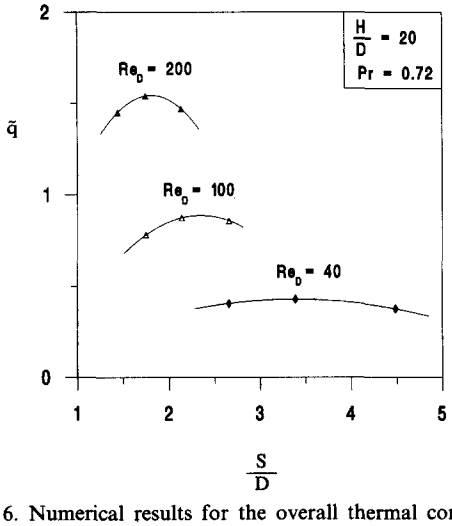

Fig. 6. Numerical results for the overall thermal conductance.

DISCUSSION

In conclusion, Fig. 3 shows that the optimal spacing decreases as the free-stream velocity (or Re_D) increases, and as the flow length of the array (H) decreases. Figure 4 shows the corresponding behavior of the maximum overall thermal conductance between the array and the coolant. These trends can be explained based on a simple order-of-magnitude argument of the same type as that used in ref. [13]. The analysis consists of determining the $S \to 0$ and $S \to \infty$ asymptotes of the function $\tilde{q}(S)$ and intersecting the asymptotes.

Consider the free-stream of velocity U_∞ and temperature T_∞, and a number of parallel cylinders oriented perpendicularly to the approaching fluid. The cylinders occupy the fixed volume $H \times L \times W$, where H is aligned with U_∞. We are interested in the cylinder-to-cylinder spacing S that maximizes the overall thermal conductance between the fixed volume and the free stream, $q/(T_w - T_\infty)$. To optimize the spacing S is equivalent to determining the optimal number of cylinders n in the fixed volume HLW, namely $n = HW/(S+D)^2 \cos 30°$, or the optimal porosity of the HLW space

$$\varphi = 1 - \frac{n(\pi/4)D^2}{HW}. \tag{10}$$

In the small-spacing limit, the cylinders almost touch, the fluid spends a long time in the HLW volume and the fluid outlet temperature is practically the same as the cylinder temperature. The total heat transfer rate between the volume and the fluid is

$$q_{smallS} = \dot{m} c_p (T_w - T_\infty) \tag{11}$$

where $\dot{m}$ is the total mass flow rate, $\dot{m} = \rho WLU$. The volume averaged longitudinal velocity U can be estimated by assuming Darcy flow:

$$U = \frac{K}{\mu}\frac{\Delta p}{H} \tag{12}$$

where the permeability of the equilateral triangle array is represented adequately by the Carman–Kozeny model [19]

$$K = \frac{D^2\varphi^3}{C(1-\varphi)^2} \tag{13}$$

where $C \sim 100$ in an order of magnitude sense. In the small-S limit the pressure difference between the front and back planes of the fixed volume, Δp, is controlled by the dynamic pressure of the approaching stream, in accordance with equation (6). Combining these equations we find that in the small-S limit the volume averaged velocity U behaves as

$$U \cong \frac{\rho U_\infty}{200\mu H} \frac{\varphi^3}{(1-\varphi)^2} \tag{14}$$

where

$$\varphi = 1 - \frac{0.907}{(1+S/D)^2}. \tag{15}$$

Since we are especially interested in the limit $S/D \to 0$ where the cylinders touch and the interstitial flow stops ($U \to 0$), we adjust equation (15) slightly by replacing 0.907 with 1, and equation (14) becomes

$$U \cong \frac{\rho U_\infty^2 D^2}{200\mu H} \frac{(\tilde{S}^2+2\tilde{S})^3}{(\tilde{S}+1)^2} \tag{16}$$

where $\tilde{S} = S/D$. Finally, we combine equation (16) with equation (11), recognize that $\tilde{S} \ll 1$, and determine the asymptote of the overall thermal conductance of the array:

$$\left(\frac{q}{T_w - T_\infty}\right)_{\text{small}S} \cong \tfrac{1}{25}\rho c_p v \frac{WL}{H} Re_D^2 \tilde{S}^3. \tag{17}$$

In the opposite extreme, $S \gg D$, each cylinder is bathed by free-stream fluid (U_∞, T_∞). The heat transfer from a single cylinder is

$$q_1 = Nu_D \frac{k}{D} \pi DL(T_w - T_\infty) \tag{18}$$

for which Zukauskas [20] recommended the correlation $Nu_D = 0.52\, Pr^{0.37}\, Re_D^{1/2}$, which is valid in the range $Pr \geqslant 0.5$ and $40 < Re_D < 1000$. Combining $q = nq_1$ with equation (18), and recognizing that $\tilde{S} \gg 1$, we obtain the large-S asymptote

$$\left(\frac{q}{T_w - T_\infty}\right)_{\text{large}S} \cong 1.89\, k \frac{HLW}{D^2} Pr^{0.37}\, Re_D^{1/2}\, \tilde{S}^{-2}. \tag{19}$$

In summary, we note that as $\tilde{S}$ increases, the thermal conductance increases when $\tilde{S}$ is small [equation (17)] and decreases when $\tilde{S}$ is large [equation (19)]. This means that the optimal spacing for maximum thermal conductance can be located *approximately* by intersecting equations (17) and (19):

$$\left(\frac{S}{D}\right)_{\text{opt}} \cong 2.2 Pr^{-0.13} \left(\frac{D}{H}\right)^{-2/5} Re_D^{-3/10}. \tag{20}$$

This relation has been plotted in Fig. 3, and is responsible for the group used on the abscissa. The trend predicted with equation (20) is the same as in the experimental and numerical data: the optimal spacing decreases noticeably as Re_D increases.

Figure 3 also shows that, as expected, the scaling result (20) agrees approximately with the experimental and numerical S_{opt}/D data. This is remarkable in view of the fact that: (a) the analytical method of intersecting the asymptotes is by definition approximate; (b) equation (20) is based on a Nu_D correlation valid only for $40 < Re_D < 1000$; and (c) in the scale analysis the cylinders were assumed to be at the same temperature, while in the experiments the cylinders had equal heat transfer rates. Point (c) strengthens a conclusion reached in ref. [13], where it was shown that in stacks of smooth plates the optimal spacing for isothermal plates is nearly the same as the optimal spacing for uniform flux plates.

An approximate estimate for the maximum overall thermal conductance that corresponds to the optimal spacing can be obtained by substituting $(S/D)_{opt}$ in either equation (17) or equation (19):

$$\tilde{q}_{max} \leqslant 0.4 Pr^{0.62} \left(\frac{D}{H}\right)^{4/5} Re_D^{11/10}. \tag{21}$$

Equation (21) with an equal sign is plotted in Fig. 4. The inequality sign in equation (21) is a reminder that the intersection of asymptotes (17) and (19) on the $\tilde{q}$–$\tilde{S}$ plane occurs *above* the true maximum of the $\tilde{q}(\tilde{S})$ curve [13]. In other words, equation (21) anticipates the scaling trends with respect to changes in (H/D) and Re_D, and provides an upper bound for the actual value of $\tilde{q}_{max}$.

These predictions are in good agreement with the alignment of the experimental and numerical data in Fig. 4. That the high-Re_D experimental data begin to deviate from the theoretical trend may be due to the fact that equation (21) is based on an empirical correlation that is not valid above $Re_D = 1000$. This deviation is actually a stimulus for further experimental studies at high Re_D values, so that the path outlined by the present data in Figs. 3 and 4 can be completed.

Acknowledgements—This work was supported by a grant from the Air Force Office of Scientific Research under the guidance of Major Dan Fant. The computational work was made possible by a grant from the Pittsburgh Supercomputing Center.

REFERENCES

1. G. P. Peterson and A. Ortega, Thermal control of electronic equipment and devices, *Adv. Heat Transfer* **20**, 181–314 (1990).
2. A. Bar-Cohen and A. D. Kraus, *Advances in Thermal Modeling of Electronic Components and Systems*, Vol. 2. ASME Press, New York (1990).
3. A. Bar-Cohen and W. M. Rohsenow, Thermally optimum spacing of vertical, natural convection cooled, parallel plates, *J. Heat Transfer* **106**, 116–123 (1984).
4. A. Bejan, *Convection Heat Transfer*, p. 157, Problem 11. Wiley, New York (1984).
5. S. H. Kim, N. K. Anand and L. S. Fletcher, Free convection between series of vertical parallel plates with embedded line heat sources, *J. Heat Transfer* **113**, 108–115 (1991).
6. N. K. Anand, S. H. Kim and L. S. Fletcher, The effect of

plate spacing on free convection between heated parallel plates, *J. Heat Transfer* **114,** 515–518 (1992).
7. R. W. Knight, J. S. Goodling and D. J. Hall, Optimal thermal design of forced convection heat sinks—analytical, *J. Electronic Packaging* **113,** 313–321 (1991).
8. R. W. Knight, J. S. Goodling and B. E. Gross, Optimal thermal design of air cooled forced convection finned heat sinks—experimental verification, *IEEE Trans. Components, Hybrids Manufacturing Technol.* **15,** 754–760 (1992).
9. A. Bejan and A. M. Morega, Optimal arrays of pin fins and plate fins in laminar forced convection, *J. Heat Transfer* **115,** 75–81 (1993).
10. M. Hirata, Y. Kakita, Y. Yada. Y. Hirose. T. Morikawa and H. Ecomoto, Temperature distribution of finned integrated circuits, *Fijitsu Sci. Technol. J.* **6,** 91–115 (1970).
11. W. Nakayama, H. Matsushima and P. Goel, Forced convective heat transfer from arrays of finned packages. In *Cooling Technology for Electronic Equipment* (Edited by W. Aung), pp. 195–210. Hemisphere, New York (1988).
12. H. Matsushima, T. Yanagida and Y. Kondo, Algorithm for predicting the thermal resistance of finned LSI packages mounted on a circuit board, *Heat Transfer—Jap. Res.* **21,** 504–517 (1992).
13. A. Bejan and E. Sciubba, The optimal spacing of parallel plates cooled by forced convection, *Int. J. Heat Mass Transfer* **35,** 3259–3264 (1992).
14. S. J. Kline and F. A. McClintock, Describing uncertainties in single-sample experiments, *Mech. Engng* **3,** Jan. 5–8 (1953).
15. Y. S. Touloukian *et al.*, *Thermophysical Properties of Matter*, TPRC, 3, 6, 11, Data Series, Purdue Research Foundation, New York (1970).
16. A. J. Fowler and A. Bejan, Forced convection in banks of inclined cylinders at low Reynolds numbers, *Int. J. Heat Fluid Flow* **15,** 90–99 (1994).
17. FIDAP, *Theoretical Manual and Examples Manual.* Fluid Dynamics International, Evanston, IL, Revision 7.0 (1994).
18. S. Mochizuki and Y. Yagi, Characteristics of vortex shedding in plate arrays. In *Flow Visualization* II (Edited by W. Merzkirch), pp. 99–103. Hemisphere, Washington, DC (1980).
19. D. A. Nield and A. Bejan, *Convection in Porous Media.* Springer, New York (1992).
20. A. Zukauskas, Convective heat transfer in cross flow. In *Handbook of Single-Phase Convective Heat Transfer* (Edited by S. Kakac, R. K. Shah and W. Aung), Chap. 6. Wiley, New York (1987).